Intermediate phases in rhombohedral Pb (Mg 1/3 Nb 2/3) 1 − x Ti x O 3 crystal

C.-S. Tu, H.-T. Chuang, S.-C. Lee, R. R. Chien, V. H. Schmidt, and H. Luo

Citation: Journal of Applied Physics **104**, 024110 (2008); doi: 10.1063/1.2956611
View online: http://dx.doi.org/10.1063/1.2956611
View Table of Contents: http://scitation.aip.org/content/aip/journal/jap/104/2?ver=pdfcov
Published by the AIP Publishing

Intermediate phases in rhombohedral $Pb(Mg_{1/3}Nb_{2/3})_{1-x}Ti_xO_3$ crystal

C.-S. Tu,[1,a)] H.-T. Chuang,[1] S.-C. Lee,[1] R. R. Chien,[2] V. H. Schmidt,[2] and H. Luo[3]
[1]*Department of Physics, Fu Jen Catholic University, Taipei 242, Taiwan*
[2]*Department of Physics, Montana State University, Bozeman, Montana 59717, USA*
[3]*Shanghai Institute of Ceramics, Chinese Academy of Sciences, Shanghai 201800, People's Republic of China*

(Received 24 March 2008; accepted 10 May 2008; published online 22 July 2008)

Phase transformations of (111)-cut $Pb(Mg_{1/3}Nb_{2/3})_{1-x}Ti_xO_3$ ($x=0.30$) single crystals before and after an electric (E)–field poling have been investigated by means of dielectric permittivity, hysteresis loop, polarization current, and *in situ* x-ray diffraction as a function of temperature. An *R-T-C* transition sequence was observed in the unpoled sample upon zero-field heating. *R*, *T*, and *C* are rhombohedral, tetragonal, and cubic phases, respectively. After a prior *E*-field poling, an extra intermediate monoclinic (possible M_A) phase was induced and the crystal underwent an *R*-M_A-*T*-*C* phase sequence with significant responses in polarization current. The dielectric dispersion was diminished after poling and reappeared in the cubic state. The dielectric permittivities with and without a prior poling were found to follow the Curie–Weiss equation, $\varepsilon' = C/(T-T_0)$, above the Burns temperature 505 K with the same constants $C=1.9\times10^5$ K and $T_0=460$ K. © *2008 American Institute of Physics*. [DOI: 10.1063/1.2956611]

I. INTRODUCTION

Polar nanostructures [or polar nanoregions (PNRs)] are possibly the most important feature in relaxor ferroelectrics because they are responsible for ferroelectric (FE) properties and phase transformations. Field-cooled and zero-field-cooled (ZFC) ^{207}Pb nuclear-magnetic-resonance spectra of the prototype relaxor $Pb(Mg_{1/3}Nb_{2/3})O_3$ (PMN) crystal showed the existence of two components—isotropic spherical glass matrix and anisotropic FE nanoclusters.[1,2] The FE polar clusters, which can respond to an external *E* field, are embedded in a single-dipole-glass matrix, which does not respond appreciably to an *E* field.[2] Neutron analysis of unpoled PMN powder shows that the volume fraction of PNRs and their correlation lengths increase drastically below 200 K.[3] Two atomic displacements (δ_{cm} and δ_{shift}) were proposed below the Burns temperature (600–650 K) in PMN by neutron diffuse scattering.[4] δ_{cm} is caused by the soft-mode condensation, and δ_{shift} represents a uniform displacement of PNRs along their polar direction relative to the surrounding cubic matrix. These phenomena indicate that PMN is an incipient FE. First-principles dynamic simulation for PMN shows the formation of nanoclusters in the quenched short-range-ordered regions below the Burns temperature.[5] By dielectric and domain studies, an incipient FE nature was found in $Pb(Mg_{1/3}Nb_{2/3})_{1-x}Ti_xO_3$ (PMN-PT) crystals, in which a "hidden" transition was enhanced by a prior poling.[6]

Ferroelastic crystals usually consist of structural twins to accommodate the spontaneous lattice distortion and minimize the elastic strain energy. A nanotwin diffraction theory was recently developed by Wang,[7,8] showing that tetragonal (*T*) nanotwins of the {101} twin plane can mimic the monoclinic M_C phase, and rhombohedral (*R*) nanotwins of {001} and {110} twin planes can mimic the monoclinic M_A and M_B phases, respectively. Since the nanodomain size is much smaller than the coherent length of diffraction radiation, scattered waves from individual nanodomains coherently superimpose in diffraction. Thus broadening of the reflection peak is expected.[8] Nanotwins of *T* phase with a domain size of about 10 nm have been observed by transmission electron microscopy in (001)-cut PMN-33%PT, which appears to be the M_C phase in polarized light microscopy.[9]

High energy x-ray diffraction (XRD) results show distinct outer layers (~10–50 μm) in $Pb(Zn_{1/3}Nb_{2/3})_{1-x}$–$Ti_xO_3$ (PZN-PT) ($x=0$, 4.5, and 8.0) crystals.[10] Both PZN-4.5%PT and PZN-8%PT have *R* phases in both the outer layer and the interior.[10] An *R* lattice was found in both the outer layer and the crystal interior with increasing Ti content (x).[10] The outer layer structure is different from the interior for a small Ti content.[11] In the $Pb(Zn_{1/3}Nb_{2/3})O_3$ (PZN) crystal, *X* and *R* phases were suggested for the interior and outer layers, respectively.[11] Similar differences between the outer layer and the interior have been reported in PMN-PT crystals.[12,13] Neutron scattering results show that PMN-10%PT and PMN-20%PT transform to phase *X* instead of *R* phase below T_C.[12] In PMN-27%PT, the low-temperature phase was found to be *R* in both the outer layer and the interior. Neutron diffraction as a function of crystal depth in PMN crystal reveals a strong lattice distortion and depth dependence in the surface region over a length scale ~100 μm.[14] These results suggest that the ground state of the PMN-PT crystal interior prefers the *X* phase for a small Ti content and transfers to the *R* phase as the Ti content increases. The *R* phase has been observed in PMN-PT even for a very small Ti content by conventional XRD, which basically probes the outer layers.[15]

For piezoelectric performance, an *E*-field poling is usually employed before application. However, how *E*-field poling affects nanostructure, FE polarization, and phase thermal stability still lacks consistent understanding of relaxor FE

[a)]Author to whom correspondence should be addressed. Electronic mail: 039611@mail.fju.edu.tw.

crystals, especially for the compounds near the morphotropic phase boundary. In the (111)-cut relaxor FE crystals containing various *B*-site elements, the dielectric permittivity after a prior poling is usually much smaller than one without poling near room temperature.[16] *E*-field-induced intermediate phases are often seen upon zero-field heating and followed by a re-entry of dielectric dispersion as temperature approaches the cubic state.[16] However, no one had explained these dramatic phenomena clearly before. In this report, two intermediate phase transitions, R-M_A and M_A-T, were observed in the prior-poled sample upon zero-field heating. A re-entry of dielectric dispersion, which is correlated to polar nanostructures, was observed while the crystal enters the cubic state. According to previous XRD results,[12,13] both the outer layer and the interior of PMN-xPT crystals ($x \geqslant 27\%$) have the same structure. Therefore, the conventional XRD study in this work can present the interior structure.

II. EXPERIMENTAL PROCEDURE

The PMN-xPT (with $x=0.30$) crystal was grown using a modified Bridgman method. A Wayne–Kerr analyzer PMA3260A was used to obtain the real part ε' of dielectric permittivity. The sample was cut perpendicular to the ⟨111⟩ direction with dimensions $5\times5\times1$ mm^3, and its basal surfaces were coated with gold electrodes. Three processes were used in the dielectric studies. The first two are called "zero field heated" (ZFH) and zero field cooled (ZFC), in which the data were taken upon heating and cooling without any poling. In "prior poled zero field heated" (PP-ZFH), the sample was poled at room temperature with a dc *E* field of 5 kV/cm along [111], then ZFH was performed without a dc *E* field. A piezoelectric resonance was seen for $f \geqslant 100$ kHz in the PP-ZFH dielectric spectra.

Two processes were used in the polarization current measurements by using a Keithley 6517A electrometer. The first one is called ZFH current density denoted by J_{ZFH} in Fig. 1(a), in which the current was taken upon zero-field heating without prior poling. In a PP-ZFH polarization current denoted by $J_{\mathrm{PP\text{-}ZFH}}$ in Fig. 1(c), the sample was poled at room temperature with a dc *E* field of 5 kV/cm along [111], then a ZFH current was performed without an *E* field. Hysteresis loops were taken by using a Sawyer–Tower circuit at $f=46$ Hz. A Janis CCS-450 cold-head was used with a Lakeshore 340 controller for temperature-dependent measurements.

A high-temperature Rigaku model MultiFlex x-ray diffractometer with Cu $K\alpha_1$ ($\lambda=0.154\,06$ nm) and Cu $K\alpha_2$ ($\lambda=0.154\,44$ nm) radiations was used for an *in situ* symmetry study of the unit cell. The intensity ratio between $K\alpha_1$ and $K\alpha_2$ radiations is about 2:1.[17] To avoid surface stress caused by polishing, thin gold films (thickness $\cong$ 30 nm) were deposited on the basal surfaces and were kept on the sample after poling. The sample thickness is 0.70 mm, and the x-ray penetration depth is less than 10 μm.[10] The XRD spectra were fitted by using the PEAKFIT software with the sum of Gaussian and Lorentzian terms. The $K\alpha_1$ and $K\alpha_2$ peaks for the same reflection should have the same separation and ratio of full width at half maximum.

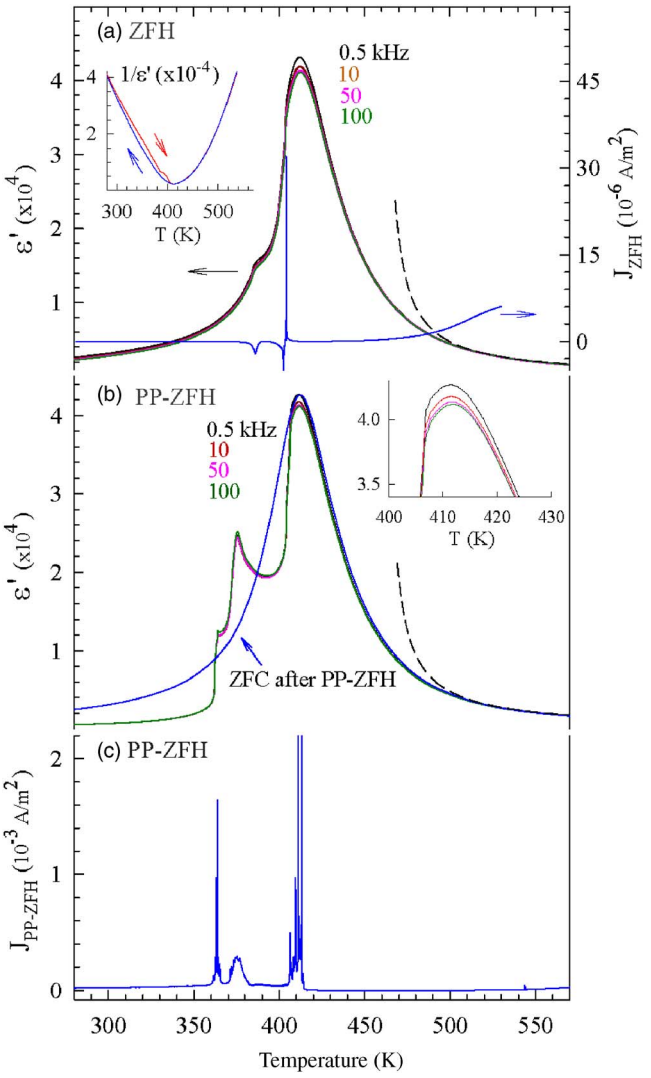

FIG. 1. (Color online) (a) ZFH dielectric permittivity $\varepsilon'_{\mathrm{ZFH}}$ and polarization current density J_{ZFH} (with the scale at the right vertical axis), (b) PP-ZFH dielectric permittivity $\varepsilon'_{\mathrm{PP\text{-}ZFH}}$, and (c) PP-ZFH polarization current density $J_{\mathrm{PP\text{-}ZFH}}$. The $1/\varepsilon'$ [inset of (a)] and $\varepsilon'_{\mathrm{ZFC}}$ after PP-ZFH were taken at $f=10$ kHz. The inset of (b) is an enlargement of $\varepsilon'_{\mathrm{PP\text{-}ZFH}}$ near T_m.

The relation of the XRD 2θ-reflection position and *d* spacing obeys the Bragg law $2d_{hkl}\sin\theta_{hkl}=n\lambda$ for both the $K\alpha_1$ and $K\alpha_2$ radiations. The *d* values for the six *T* domain types are $1/d^2=(h^2+k^2)/a^2+(l^2/c^2)$, where (h,k,l) and (a,b,c) are domain crystallographic orientation and lattice parameters, respectively. For the (111) orientation, *h*, *k*, and *l* independently take on the values ±1, so $1/d^2=2/a^2+1/c^2$ for all *T* domains.[17] For the eight *R* domain types, the same *h*, *k*, and *l* values apply. The two domains for which *h*, *k*, and *l* all have the same sign give one *d* spacing, whereas the other six give another *d* spacing, according to the following relation: $1/d^2=[(h^2+k^2+l^2)\sin^2\alpha+2(hk+kl+hl)(\cos^2\alpha-\cos\alpha)]/[a^2(1-3\cos^2\alpha+2\cos^3\alpha)]$.[17] The unit cell of FE orthorhombic (O) domains seen in FE perovskite is canted at 45° to the C cell and has lattice constants $a\cong b\cong\sqrt{2}a_{\mathrm{cub}}$ and $c\cong a_{\mathrm{cub}}$. The 12 O domain types have two *d* spacings, six given by $1/d^2=4/a^2+1/c^2$ and six by $1/d^2=4/b^2+1/c^2$. These *d* spacings are based on the relation $1/d^2=(h^2/a^2)$

$+(k^2/b^2)+(l^2/c^2)$,[17] where for this crystal cut and unit cell we have ($h=\pm 2$, $k=0$, $l=\pm 1$) or ($h=0$, $k=\pm 2$, $l=\pm 1$), with the $\pm$ signs all independent.

III. RESULTS AND DISCUSSION

Figure 1 shows (a) ZFH dielectric permittivity and polarization current density J_{ZFH}, (b) PP-ZFH dielectric permittivity, and (c) polarization current density $J_{\mathrm{PP\text{-}ZFH}}$ after a prior poling of $E=5.0$ kV/cm. The dielectric maxima (associated with frequency dispersion) and corresponding temperatures ($T_m \cong 410$ K) are nearly the same in both ZFH and PP-ZFH. The ZFH dielectric permittivity $\varepsilon'_{\mathrm{ZFH}}$ exhibits a step-up-like anomaly and a steep-rise shoulder (where a noticeable frequency dispersion begins to appear) near 385 and 403 K, respectively. The ZFH polarization current density J_{ZFH} shows two discontinuous responses, respectively, in the regions of 380–390 and 400–405 K, which are consistent with two thermal hystereses in the regions of 280–380 and 380–405 K, as shown in the inset of Fig. 1(a), implying two first-order phase transformations. These J_{ZFH} current responses consisting of two downward spikes and an upward spike, are associated with spontaneous polarization P_S of randomly oriented domains, i.e., $J_{\mathrm{ZFH}}=-\partial P_S/\partial t$. These domains must form gradually upon cooling because there is no anomaly seen in the ZFC process, as seen in the inset of Fig. 1(a).

The PP-ZFH dielectric permittivity $\varepsilon'_{\mathrm{PP\text{-}ZFH}}$ exhibits three sharp anomalies near 363, 375, and 405 K. It is important to note that at room temperature $\varepsilon'_{\mathrm{PP\text{-}ZFH}} \cong 660$ is much smaller than $\varepsilon'_{\mathrm{ZFH}} \cong 2880$ for measuring frequency $f=10$ kHz. This significant reduction indicates that the prior E-field poling along [111] enhances the [111] R phase that should have no polarization rotation under a [111] measuring field and thus exhibits small permittivity. The depolarization current density $J_{\mathrm{PP\text{-}ZFH}}$ after a prior poling at $E=5.0$ kV/cm shows three positive peaks and is consistent with three corresponding anomalies in $\varepsilon'_{\mathrm{PP\text{-}ZFH}}$. This depolarization current density $J_{\mathrm{PP\text{-}ZFH}}$ is associated with the decay of the E-field-induced polarization P_{ind}, i.e., $J_{\mathrm{PP\text{-}ZFH}}=-\partial P_{\mathrm{ind}}/\partial t$.

The dielectric dispersion was depressed after a prior poling, as seen in Fig. 1(b) until $T_{\mathrm{re}}=405$ K, where the dielectric dispersion reappears completely, associated with a strong multiple-peak response in depolarization current [Fig. 1(c)]. Multiple spikes of depolarization current can be interpreted as discrete changes in the size or rotation of FE microdomains or nanodomains. Here we define T_{re} as the temperature above which the dielectric dispersion recovers upon zero-field heating after a prior-poling at room temperature. Our $\varepsilon'_{\mathrm{PP\text{-}ZFH}}$ and depolarization current responses are similar to the dielectric and discharging results of the (111) poled PMN-30%PT crystal,[16] in which an R (macrodomain)-R (microdomain)–T-C phase sequence was proposed upon zero-field heating.

Both $\varepsilon'_{\mathrm{ZFH}}$ and $\varepsilon'_{\mathrm{PP\text{-}ZFH}}$ were found to follow the Curie–Weiss equation, $\varepsilon'=C/(T-T_0)$, above 505 K, below which there is a noticeable deviation from the Curie–Weiss law. The dashed lines in Figs. 1(a) and 1(b) are fittings with the same constants $C=1.9\times 10^5$ K and $T_0=460$ K for both $\varepsilon'_{\mathrm{ZFH}}$ and $\varepsilon'_{\mathrm{PP\text{-}ZFH}}$. We consider 505 K to be the Burns temperature (T_B), below which dipole glass attenuated dielectric response and polar nanoclusters begin to develop.[4] The weaker dielectric response of a dipole glass causes deviation from the Curie–Weiss law, and the polar nanocluster dynamics are responsible for the dielectric dispersion.[18] As given in Fig. 1(b), the ZFC dielectric permittivity measured after the PP-ZFH process shows a similar behavior as seen in $\varepsilon'_{\mathrm{ZFC}}$ [in the inset of Fig. 1(a)] and has the same Burns temperature. This indicates that the polarized state induced by an E field can be erased by thermal annealing.

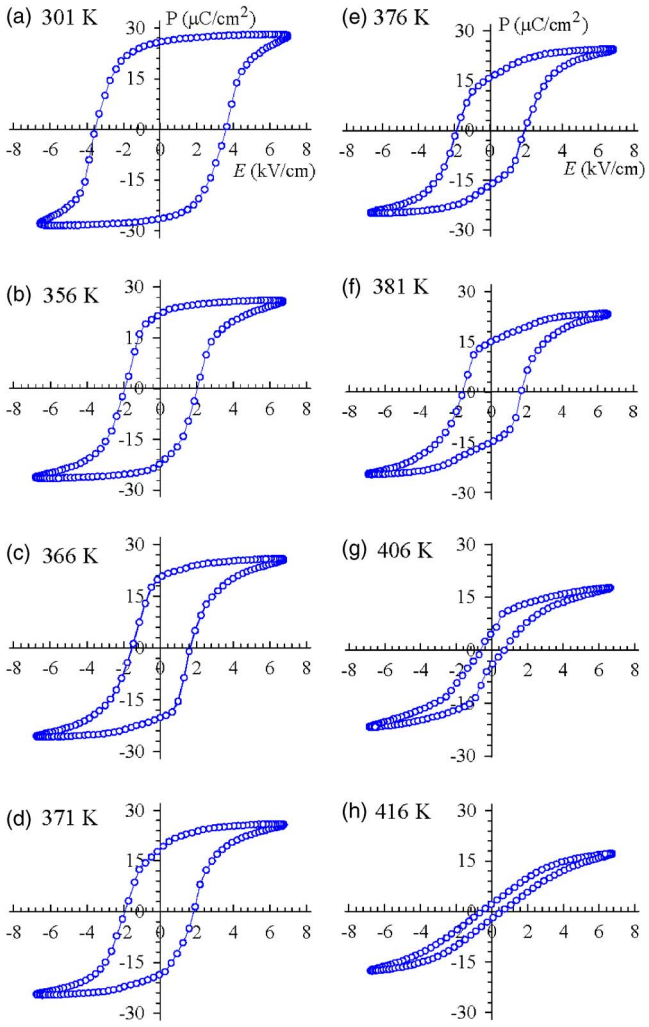

FIG. 2. (Color online) Temperature-dependent hysteresis loops upon heating.

Figures 2 and 3 show temperature-dependent hysteresis loops, and remanent polarization (P_r) and coercive field (E_C), respectively. P_S, P_r, and E_C are about 28.0 μC/cm^2, 26 μC/cm^2, and 3.6 kV/cm at room temperature, respectively. E_C and P_r exhibit a local minimum and a steep decline near 363 K, respectively. As temperature increases, E_C reaches a local maximum and P_r shows an obvious change in slope near 375 K. The polarization appears to retain some finite magnitude even above $T_m \cong 410$ K, as seen commonly in disordered materials, but this could result from a field-induced transition or from the finite measuring frequency of 46 Hz. These phenomena are consistent with dielectric

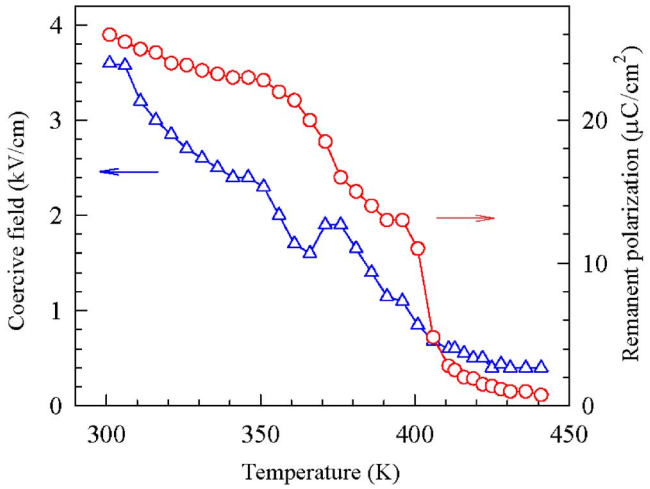

FIG. 3. (Color online) Temperature-dependent remanent polarization (P_r) and coercive field (E_C) upon heating.

anomalies in $\varepsilon'_{\text{PP-ZFH}}$ [Fig. 1(b)] and the positive responses of polarization current in Fig. 1(c). Three positive polarization current responses near 363, 375, and 410 K can be explained by the negative slopes of polarization in the corresponding temperature regions, as seen in Fig. 3, i.e., $J_{\text{PP-ZFH}}=-\partial P_{\text{ind}}/\partial t$.

The ZFH (111) XRD spectra are given in Fig. 4. At room temperature, the XRD shows two peaks, which correspond to the two (111) and the six $(\bar{1}\bar{1}1)$ and $(\bar{1}11)$ type *R* reflections from different oriented *R* domains. Note that $(\bar{1}\bar{1}1)$ and $(\bar{1}11)$ reflections have the same *d* spacing for the *R* phase. As seen in Fig. 5, the *R* phase was confirmed by the $1/\sqrt{3}$ ratio between spontaneous polarizations $P_S \cong 16.0\ \mu\text{C/cm}^2$ and $P_S \cong 28.0\ \mu\text{C/cm}^2$ taken respectively along [001] and [111] at room temperature. $1/\sqrt{3}$ is the projection fraction of the [111] polarization on the [001] axis. Figure 6(b) shows the temperature-dependent lattice parameter and α angle of the *R* unit cell determined from two *d* spacings of $K\alpha_1$ reflections. The lattice constant and the α angle of the *R* phase are $a_R = 4.0275$ Å and $\alpha = 89.906°$ at room temperature.

As temperature increases, as shown in Figs. 4 and 6, the two different *d* spacings of the *R* phase gradually approach each other but then jump to join together near 385 K, indicating a first-order phase transition. This is consistent with the current spikes near 385 K seen in Fig. 1(a). A single *d* spacing was observed above 385 K and remains almost constant until 403 K, as shown in Fig. 6(a). The phase transition near 385 K is *R*-*T* because the angle α of *R* unit cell moves toward 90° near 385 K, as seen in Fig. 6(b). Note that (100), (010), and (001) *T* reflections have the same *d* spacing in the (111) XRD, i.e., $1/d^2 = 2/a^2 + 1/c^2$. Above 403 K, as shown in Figs. 4 and 6, the *d* spacing gradually rises due to thermal expansion. No obvious discontinuity in *d* spacing is seen at 403 K, but none is expected for a (111) reflection even for a first-order *T*-*C* phase transition if the cell volume is unchanged by the transition. The first-order *T*-*C* transition is confirmed by $\varepsilon'_{\text{ZFH}}$ and the polarization current density J_{ZFH}, which exhibit a steep rise and a discontinuous downward-and-upward spike near 403 K, respectively. Above 403 K the dielectric dispersion becomes much more noticeable and

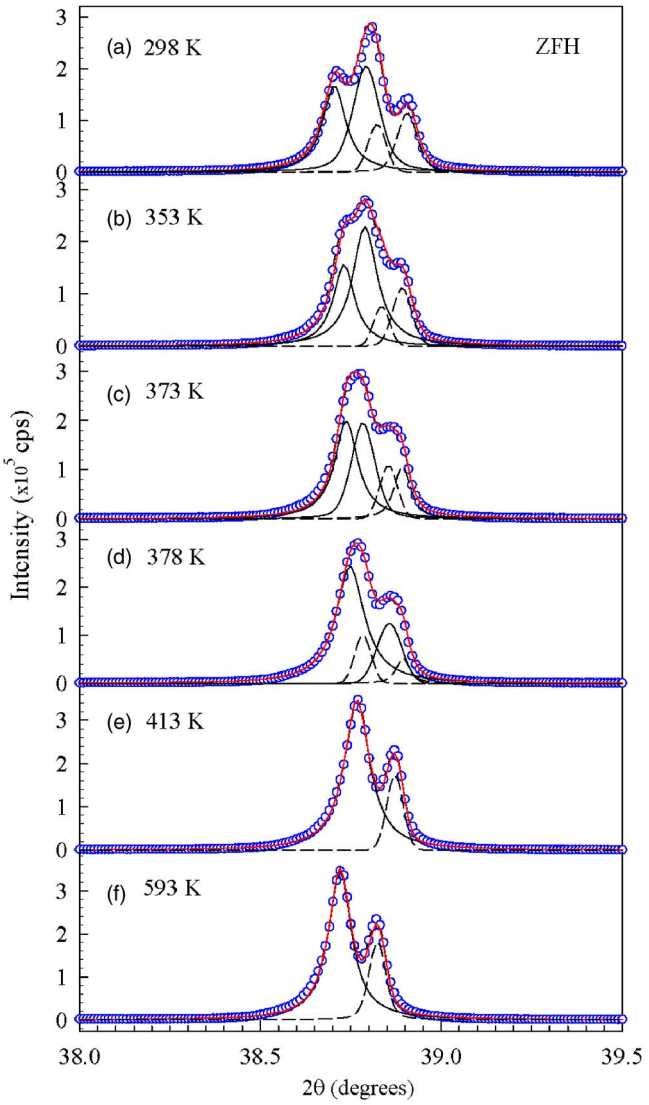

FIG. 4. (Color online) ZFH XRD spectra. The solid and short-dashed lines correlate to the $K\alpha_1$ and $K\alpha_2$ radiations, respectively. The red solid line is the sum of fitting curves.

then gradually vanishes as the Burns temperature $T_B = 505$ K is approached. Figure 6 gives the temperature dependences of *d* spacing and lattice parameters in the ZFH process. In brief, the unpoled crystal follows an *R*-*T*-*C* transition sequence near 385 and 403 K upon zero-field heating. Note that the *T*-*C* transition does not occur at the dielectric maximum temperature $T_m \cong 410$ K.

PP-ZFH XRD spectra and temperature-dependent *d* spacing after a prior poling along [111] are given in Figs. 7 and 8. At room temperature, the (111) XRD shows a single peak, which corresponds to the (111) *R* reflection due to the disappearance of differently oriented *R* domains by the prior *E*-field poling along [111]. As temperature increases, as shown in Fig. 8, the PP-ZFH (111) XRD spectra does not exhibit an obvious discontinuity near 363 K, where $\varepsilon'_{\text{PP-ZFH}}$ [Fig. 1(b)] and $J_{\text{PP-ZFH}}$ [Fig. 1(c)] indicate a first-order phase transition. A single XRD peak was observed at 366 K from the (111) reflection and indicates that the phase is not orthorhombic (*O*), which should have two *d* spacings from the (111) reflection.[17] In addition, from hysteresis loops as

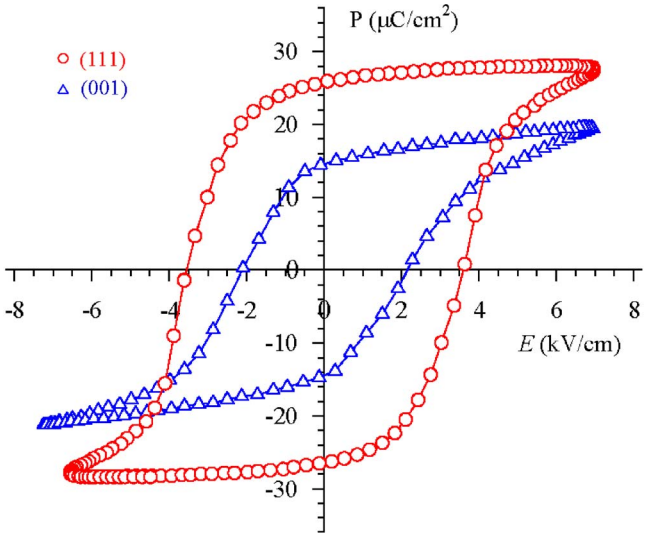

FIG. 5. (Color online) Hysteresis loops obtained from the (001) and (111) oriented crystals at room temperature.

shown in Fig. 2, the spontaneous polarizations at 366 and 298 K are respectively about 24.0 and 27.0 $\mu C/cm^2$ and have a ratio of $24/27 \cong 0.89$. The projection fraction of polarization for the [110] O phase on the [111] axis is $\sqrt{2/3} \cong 0.816$. This indicates that the structure is not likely an *O* phase in the region of 363–375 K.

What is the nature of the phase seen in PP-ZFH between 363 and 375 K? One possibility is M_A, which would provide a polarization *P* oriented between that for R_{111} and one of the three *T* domains with a *P* component along [111]. M_A domains should give XRD splittings if all domain orientations are present, but not if only those domains that have the largest *P* component along [111] occur. It is important to note that the XRD linewidth is larger at 373 K than for the adjacent ones shown in Fig. 7, namely, 30% larger than for 353 K and 20% larger than for 413 K. This could result from a spread in *P* directions lying in a plane between [111] and, for instance, [001]. According to the eighth-order Devonshire theory analysis by Vanderbilt and Cohen,[19] the *R*-M_A transition should be of first order, which may explain why discontinuities (or spikes) appear in $\varepsilon'_{\text{PP-ZFH}}$ and $J_{\text{PP-ZFH}}$ near 363 K. It is important to note that *R* nanotwins (R_{NT}) can mimic M_A and also cause a broadening of the diffraction peak due to coherent superimposition of scattered waves from individual nanodomains.[8] However, *R*-R_{NT} transition is of second order, which is not supported by discontinuities (or spikes) seen in $\varepsilon'_{\text{PP-ZFH}}$ and $J_{\text{PP-ZFH}}$ near 363 K.

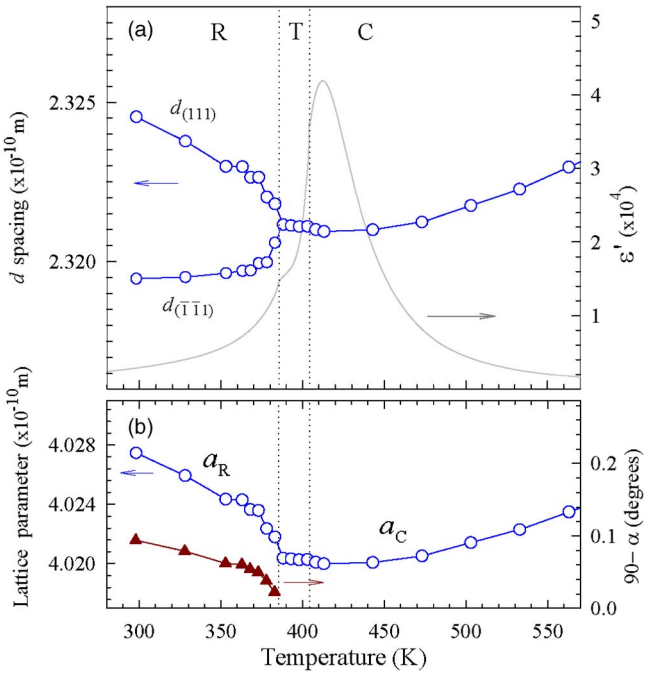

FIG. 6. (Color online) Temperature-dependent (a) *d* spacing and (b) lattice parameter obtained from the (111) XRD upon zero-field heating. The solid-line background is $\varepsilon'_{\text{ZFH}}$ for comparison. The dotted lines indicate transition temperatures.

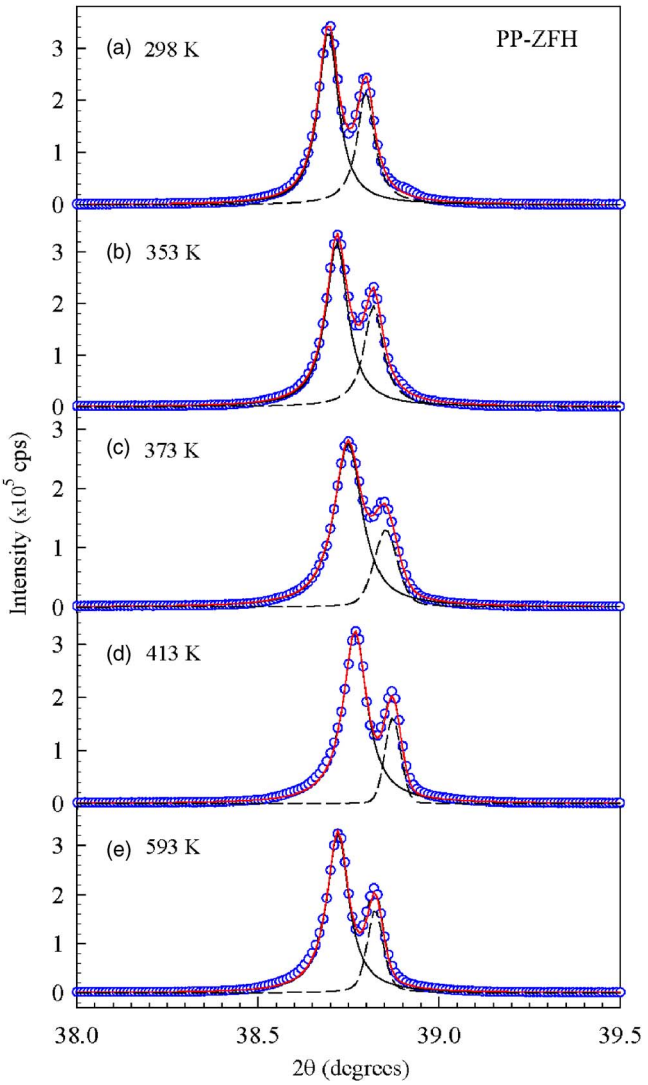

FIG. 7. (Color online) PP-ZFH XRD spectra after poling at $E=5$ kV/cm. The solid and short-dashed lines correlate to the $K\alpha_1$ and $K\alpha_2$ radiations, respectively.

As temperature increases, as seen in Fig. 8, the PP-ZFH *d* spacing exhibits a turn in slope near 375 K, which is consistent with the intermediate peak in $\varepsilon'_{\text{PP-ZFH}}$ (Fig. 1(b)). The positive broad maximum response of polarization current in the region of 370–380 K implies a second-order transition. From Fig. 2, the spontaneous polarizations at 376 and 298 K

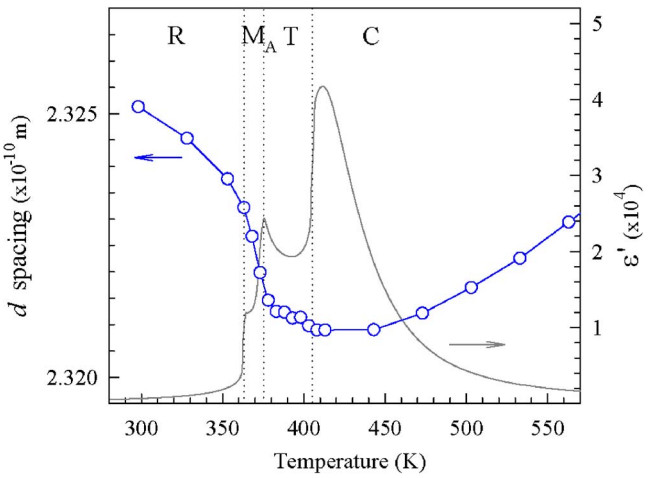

FIG. 8. (Color online) d spacing vs temperature calculated from the (111) XRD upon zero-field heating after a prior poling (E=5 kV/cm). The solid-line background is $\varepsilon'_{\text{PP-ZFH}}$ for comparison. The dotted lines indicate transition temperatures.

are respectively about 21.0 and 28.0 μC/cm^2, and the ratio is about 0.75, which is reasonably close to the $1/\sqrt{3}$ between T and R spontaneous polarizations measured along [111]. "$1/\sqrt{3}$" is the projection fraction of the [001] T polarization on the [111] axis. Thus, the transition near 375 K should be M_A-T, which is of second order according to the eighth-order Devonshire theory analysis.[19] This may explain why no obvious discontinuity appears in $J_{\text{PP-ZFH}}$ and a lattice parameter near 375 K, as seen in Figs. 1(c) and 8. As temperature increases, as shown in Figs. 7 and 8, the d spacing exhibits a sudden change in slope near 405 K and then gradually rises upon heating, suggesting a first-order T-C phase transition at 405 K. Note that $\varepsilon'_{\text{PP-ZFH}}$ exhibits a very steep increase near 405 K and $J_{\text{PP-ZFH}}$ exhibits a discontinuous response of multiple positive spikes in the region of 405–415 K, confirming a first-order T-C transition. Above 405 K the dielectric dispersion re-establishes completely and then gradually disappears as the Burns temperature T_B=505 K is approached, just as for ZFH. Figure 8 gives the temperature dependence of d spacing in the PP-ZFH process. In brief, the prior-poled crystal has an R-M_A-T-C transition sequence near 363, 375, and 405 K, respectively, upon zero-field heating.

IV. CONCLUSIONS

For a (111)-cut unpoled PMN-30%PT crystal, an R-T-C phase sequence was observed near 385 and 403 K upon zero-field heating. After a prior poling with E=5.0 kV/cm at room temperature, an extra intermediate monoclinic phase (perhaps M_A) was induced and the crystal underwent an R-M_A-T-C phase sequence upon zero-field heating. The dielectric permittivity $\varepsilon'_{\text{PP-ZFH}}$ was significantly reduced after a prior E-field poling along [111], indicating that the poling process enhances the [111] R phase that reacts to weak polarization rotation under a [111] measuring field. $\varepsilon'_{\text{PP-ZFH}}$ shows a re-entry of dielectric dispersion at T_{re}=405 K, associated with the development of polar nanostructures. Both $\varepsilon'_{\text{ZFH}}$ and $\varepsilon'_{\text{PP-ZFH}}$ were found to follow the Curie–Weiss equation, $\varepsilon'=C/(T-T_0)$, with the same constants C=1.9 $\times 10^5$ K and T_0=460 K above the Burns temperature of 505 K.

The phase sequence R-M_A-T-C in the PP-ZFH process is however different from the R (macrodomain)–R (microdomain)–T-C phase sequence proposed in the literature for the (111)-cut PMN-30%PT crystal upon zero-field heating after poling with E=15 kV/cm from the dielectric maximum temperature (T_m) to room temperature.[16] Nanotwin structures, which have played an important role during the phase transformations in a (001) oriented PMN-30%PT crystal,[20] were not obviously evidenced in this (111)-cut crystal. This may imply that the elastic strain energy (due to the spontaneous lattice distortion) in the (111)-cut rhombohedral crystal is less than that in the (001)-cut crystal.

ACKNOWLEDGMENTS

This work was supported by the National Science Council of Taiwan (Grant No. 96-2112-M-030-001).

[1] R. Blinc, V. V. Laguta, and B. Zalar, Phys. Rev. Lett. **91**, 247601 (2003).
[2] R. Blinc, V. V. Laguta, B. Zalar, and J. Banys, J. Mater. Sci. **41**, 27 (2006).
[3] I. K. Jeong, T. W. Darling, J. K. Lee, T. Proffen, R. H. Heffner, J. S. Park, K. S. Hong, W. Dmowski, and T. Egami, Phys. Rev. Lett. **94**, 147602 (2005).
[4] K. Hirota, Z.-G. Ye, S. Wakimoto, P. M. Gehring, and G. Shirane, Phys. Rev. B **65**, 104105 (2002).
[5] S. Tinte, B. P. Burton, E. Cockayne, and U. V. Waghmare, Phys. Rev. Lett. **97**, 137601 (2006).
[6] C.-S. Tu, R. R. Chien, F.-T. Wang, V. H. Schmidt, and P. Han, Phys. Rev. B **70**, 220103(R) (2004).
[7] Y. U. Wang, Phys. Rev. B **74**, 104109 (2006).
[8] Y. U. Wang, Phys. Rev. B **76**, 024108 (2007).
[9] H. Wang, J. Zhu, N. Lu, A. A. Bokov, Z. G. Ye, and X. W. Zhang, Appl. Phys. Lett. **89**, 042908 (2006).
[10] G. Xu, H. Hiraka, G. Shirane, and K. Ohwada, Appl. Phys. Lett. **84**, 3975 (2004).
[11] G. Xu, Z. Zhong, Y. Bing, Z.-G. Ye, C. Stock, and G. Shirane, Phys. Rev. B **67**, 104102 (2003).
[12] P. M. Gehring, W. Chen, Z.-G. Ye, and G. Shirane, J. Phys.: Condens. Matter **16**, 7113 (2004).
[13] G. Xu, D. Viehland, J. F. Li, P. M. Gehring, and G. Shirane, Phys. Rev. B **68**, 212410 (2003).
[14] K. H. Conlon, H. Luo, D. Viehland, J. F. Li, T. Whan, J. H. Fox, C. Stock, and G. Shirane, Phys. Rev. B **70**, 172204 (2004).
[15] Z.-G. Ye, Y. Bing, J. Gao, A. A. Bokov, P. Stephens, B. Noheda, and G. Shirane, Phys. Rev. B **67**, 104104 (2003).
[16] Z. Feng, X. Zhao, and H. Luo, J. Appl. Phys. **100**, 024104 (2006).
[17] B. D. Cullity, *Elements of X-Ray Diffraction*, 2nd edition (Addison-Wesley, Reading, MA, 1978), pp. 8–10 and 501.
[18] D. Viehland, S. J. Jang, L. E. Cross, and M. Wuttig, Phys. Rev. B **46**, 8003 (1992).
[19] D. Vanderbilt and M. H. Cohen, Phys. Rev. B **63**, 094108 (2001).
[20] C.-S. Tu, C.-M. Hsieh, R. R. Chien, V. H. Schmidt, F.-T. Wang, and W. S. Chang, J. Appl. Phys. **103**, 074117 (2008).